Supplementary information

Local administration of regulatory T cells promotes tissue healing

Bhavana Nayer[1], Jean L. Tan[1], Yasmin K. Alshoubaki[1], Yen-Zhen Lu[1], Julien M.D. Legrand[1], Sinnee Lau[1], Nan Hu[1], Anthony J. Park[1], Xiao-Nong Wang[2], Daniela Amann-Zalcenstein[3,4], Peter F. Hickey[3,4], Trevor Wilson[5], Gisela A. Kuhn[6], Ralph Müller[6], Ajithkumar Vasanthakumar[7,8,9], Shizuo Akira[10], Mikaël M. Martino[1,10,11].

[1]European Molecular Biology Laboratory Australia, Australian Regenerative Medicine Institute, Monash University, Melbourne, VIC, Australia

[2]Translational and Clinical Research Institute, Newcastle University, Newcastle upon Tyne, UK

[3]Advanced Genomics Facility, Advanced Technology and Biology Division, The Walter and Eliza Hall Institute of Medical Research, Parkville, VIC, Australia

[4]Department of Medical Biology, University of Melbourne, Melbourne, VIC, Australia

[5]MHTP Medical Genomics Facility, Monash Health Translation Precinct, Clayton, VIC, Australia

[6]Institute for Biomechanics, ETH Zurich, Zurich, Switzerland

[7]Olivia Newton-John Cancer Research Institute, Heidelberg, VIC, Australia

[8]La Trobe University, Bundoora, VIC, Australia

[9]Department of Microbiology and Immunology, The University of Melbourne, Parkville, VIC, Australia

[10]Laboratory of Host Defense, World Premier Institute Immunology Frontier Research Center, Osaka University, Osaka, Japan

[11]Victorian Heart Institute, Monash University, Melbourne, VIC, Australia

Correspondence: mikael.martino@monash.edu

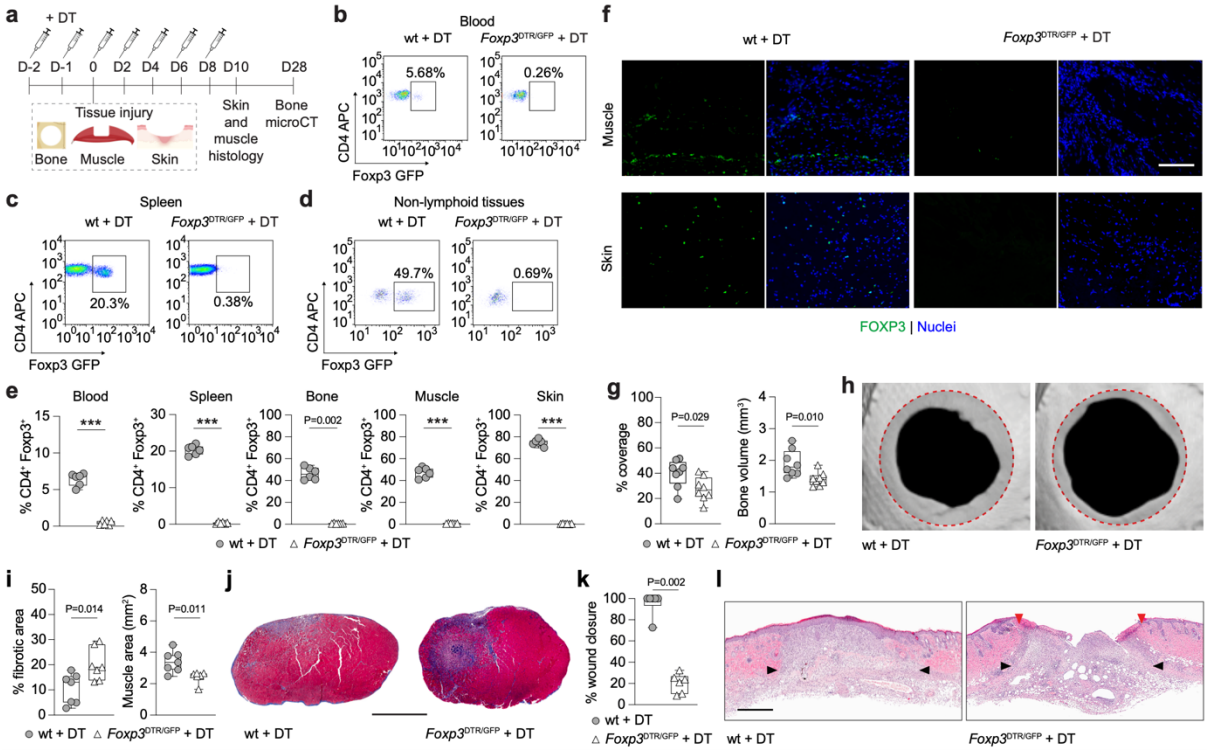

Supplementary Fig. 1: Inducible depletion of Tregs worsens tissue healing outcomes following acute bone, muscle and skin injuries. a, Experimental design for assessing tissue healing after Treg depletion. Wildtype (wt) C57BL6/J and *Foxp3*$^{DTR/GFP}$ mice were treated with diphtheria toxin (DT) starting two days prior to injury, and every other day post-injury until D8 to deplete Tregs in *Foxp3*$^{DTR/GFP}$ mice. **b-e**, Treg depletion assessed via flow cytometry on D7 post-injury. Representative flow cytometry plots of blood (**b**), spleen (**c**), and injured non-lymphoid tissues (shown here for muscle) (**d**), along with the percentage of CD4$^+$, Foxp3$^+$ Tregs (out of total CD4$^+$ T cells) in these tissues in (**e**) (*n* = 6 mice). **f**, Representative immunostaining of injured muscle and skin sections for FOXP3 in green (Tregs) and nuclei in blue at D7 post-injury in wt and *Foxp3*$^{DTR/GFP}$ mice treated with DT. Scale bar: 100 µm. **g-l**, Critical-size cranial defects, quadriceps volumetric muscle loss defect (by biopsy punch) or full-thickness dorsal skin wounds (non-splinted) were performed in wt or *Foxp3*$^{DTR/GFP}$ mice treated with DT. Tissue healing was assessed at different time points for each tissue. **g**, Bone regeneration evaluated by microCT analysis of cranial defects expressed as defect coverage and new bone volume at D28 post-injury (*n* = 8 defects). **h**, Representative cranial reconstructions. The original defect area is shaded with a dashed red outline. **i**, Muscle regeneration represented by the percentage of fibrotic-like tissue and muscle area measured by histomorphometric analysis of tissue sections at D10 post-injury (*n* = 7 defects). **j**, Representative muscle histology of a transverse section of the rectus femoris stained with Masson's trichrome at D10 post-injury. Muscle tissue is stained in red and the fibrotic-like area is in blue. Scale bar = 1 mm. **k**, Percentage wound closure at D10 post-injury evaluated by

histomorphometric analysis of tissue sections (n = 6 wounds). **l**, Representative histology of skin tissue at D10 post-injury stained with haematoxylin and eosin. Black arrows indicate wound edges and red arrows indicate tips of epithelium tongue. The epithelium (if any) is stained in purple, underneath which the granulation tissue is stained in pink-violet, with dark purple granulocyte nuclei. Scale bar = 1 mm. Data are plotted in box plots showing the median (central line) and IQR (bounds) with whiskers extending to the minimum and maximum values. Two-tailed unpaired Student's *t*-test was used in (e: Blood, Spleen, Muscle, Skin, g, i: left) and Mann Whitney U Test for non-parametric data was used in (e: Bone, i: right, k). *P* values are indicated; ***$P \leq 0.001$. Panel (**a**) created with BioRender.com released under a Creative Commons Attribution-NonCommercial-NoDerivs 4.0 International license (https://creativecommons.org/licenses/by-nc-nd/4.0/deed.en).

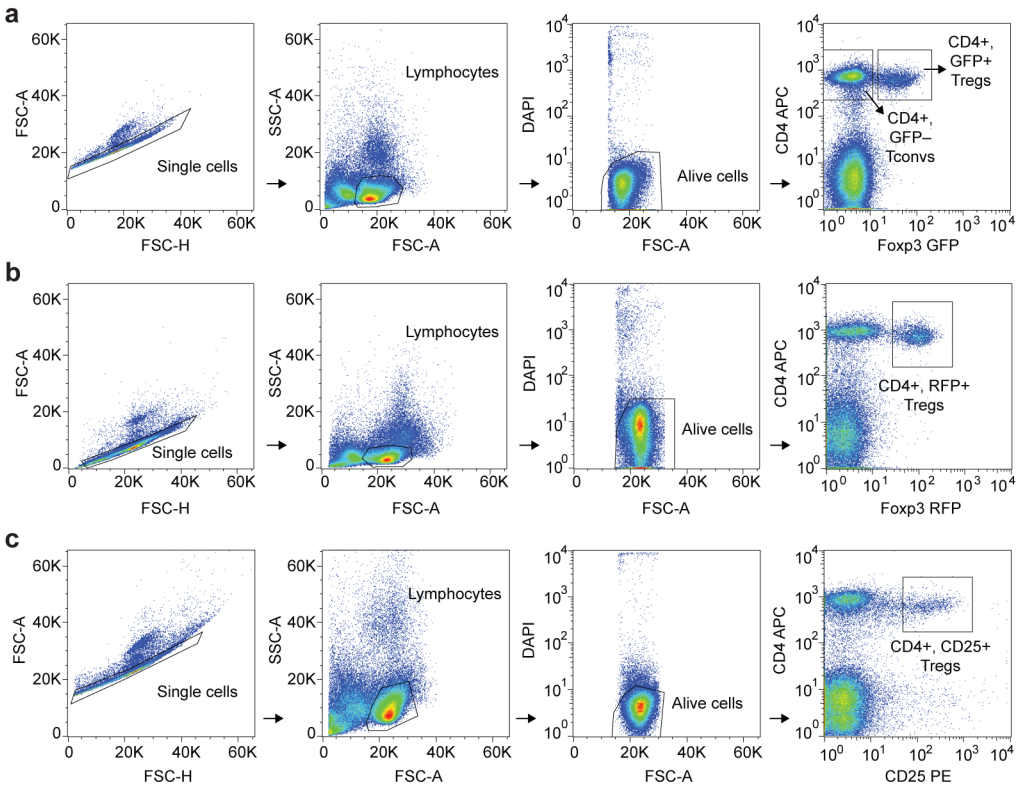

Supplementary Fig. 2: Representative flow cytometry gating strategies for sorting T cells from spleen. a-c, Gating strategy for sorting Tregs from healthy mouse spleens for all T cell delivery experiments, including $CD4^+$, GFP^+ Tregs and $CD4^+$, GFP^- Tconvs from *Foxp3*$^{DTR/GFP}$ mice (**a**), $CD4^+$, RFP^+ Tregs from *Foxp3*$^{IRES-RFP}$ mice (**b**) and $CD4^+$, $CD25^+$ Tregs from *Il10*$^{-/-}$ mice (**c**).

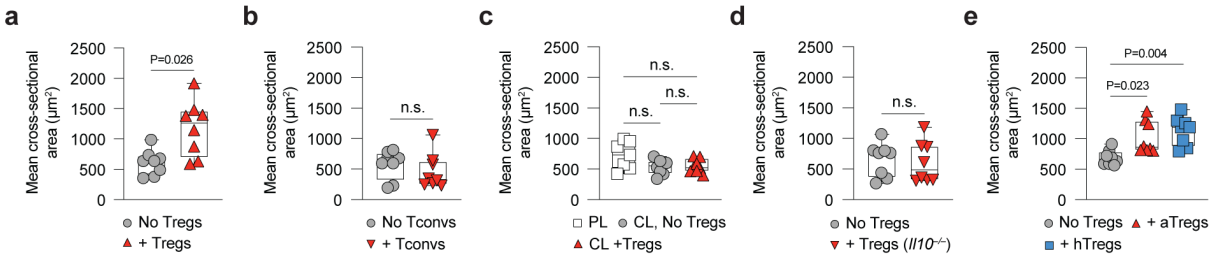

Supplementary Fig. 3: Muscle fibre cross-sectional area for all T cell delivery experiments. Average cross-sectional muscle fibre areas of individual centrally nucleated muscle fibres on sections from mice across all treatment groups, including Tregs versus control (**a**), Tconvs versus control (**b**), PBS or clodronate liposomes with/without Tregs (**c**), *Il10*$^{-/-}$ Tregs versus control (**d**) and allogeneic and human Tregs versus control (**e**). Data are plotted in box plots showing the median (central line) and IQR (bounds) with whiskers extending to the minimum and maximum values. Two-tailed unpaired Student's *t*-test was used in (**a, d**) and Mann Whitney U Test for non-parametric data was used in (**b**). One-way ANOVA with Bonferroni *post hoc* test was used in (**c**) and Kruskal-Wallis with Dunn's *post hoc* test was used for non-parametric data in (**e**) for multiple comparisons. *P* values are indicated; ***$P \leq 0.001$; n.s. indicates non-significant. (PL: PBS/ control liposomes; CL: Clodronate liposomes; aTregs: allogeneic Tregs; hTregs: human Tregs).

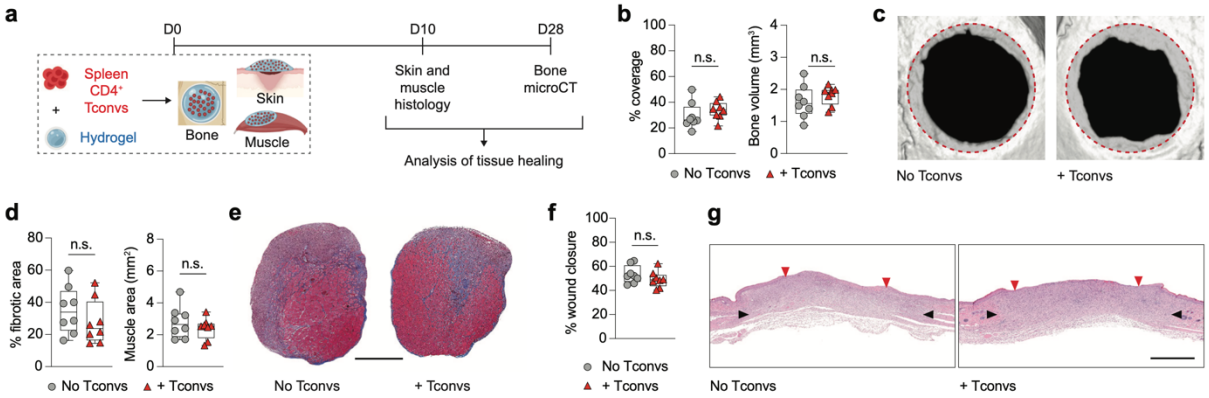

Supplementary Fig. 4: Local delivery of exogenous CD4$^+$ Tconvs does not promote tissue healing. a, Critical-size cranial defects, quadriceps volumetric muscle loss defect or full-thickness dorsal skin wounds were performed in wildtype C57BL6/J mice and treated with a fibrin hydrogel only, or hydrogel containing exogenous spleen CD4$^+$ Tconvs. Tissue healing was assessed at different time points for each tissue. **b**, Bone regeneration evaluated by microCT analysis of cranial defects expressed as defect coverage and new bone volume at D28 post-injury (*n* = 8 defects). **c**, Representative cranial reconstructions. The original defect area is shaded with a dashed red outline. **d**, Muscle regeneration represented by the percentage of fibrotic-like tissue and muscle area measured by histomorphometric analysis of tissue sections at D10 post-injury (*n* = 8 defects). **e**, Representative muscle histology of a transverse section of the rectus femoris stained with Masson's trichrome at D10 post-injury. Muscle tissue is stained in red and the fibrotic-like area is in blue. Scale bar = 1 mm. **f**, Percentage wound closure at D10 post-injury evaluated by histomorphometric analysis of tissue sections (*n* = 8 to 12 wounds). **g**, Representative histology of skin tissue stained with haematoxylin and eosin at D10 post-injury. Black arrows indicate wound edges and red arrows indicate tips of epithelium tongue. The epithelium (if any) is stained in purple, underneath which the granulation tissue is stained in pink-violet, with dark purple granulocyte nuclei. Scale bar = 1 mm. Data are plotted in box plots showing the median (central line) and IQR (bounds) with whiskers extending to the minimum and maximum values. Two-tailed unpaired Student's *t*-test was used in (**b, d, f**). *P* values are indicated; ***$P \leq 0.001$. Panel (**a**) created with BioRender.com released under a Creative Commons Attribution-NonCommercial-NoDerivs 4.0 International license (https://creativecommons.org/licenses/by-nc-nd/4.0/deed.en).

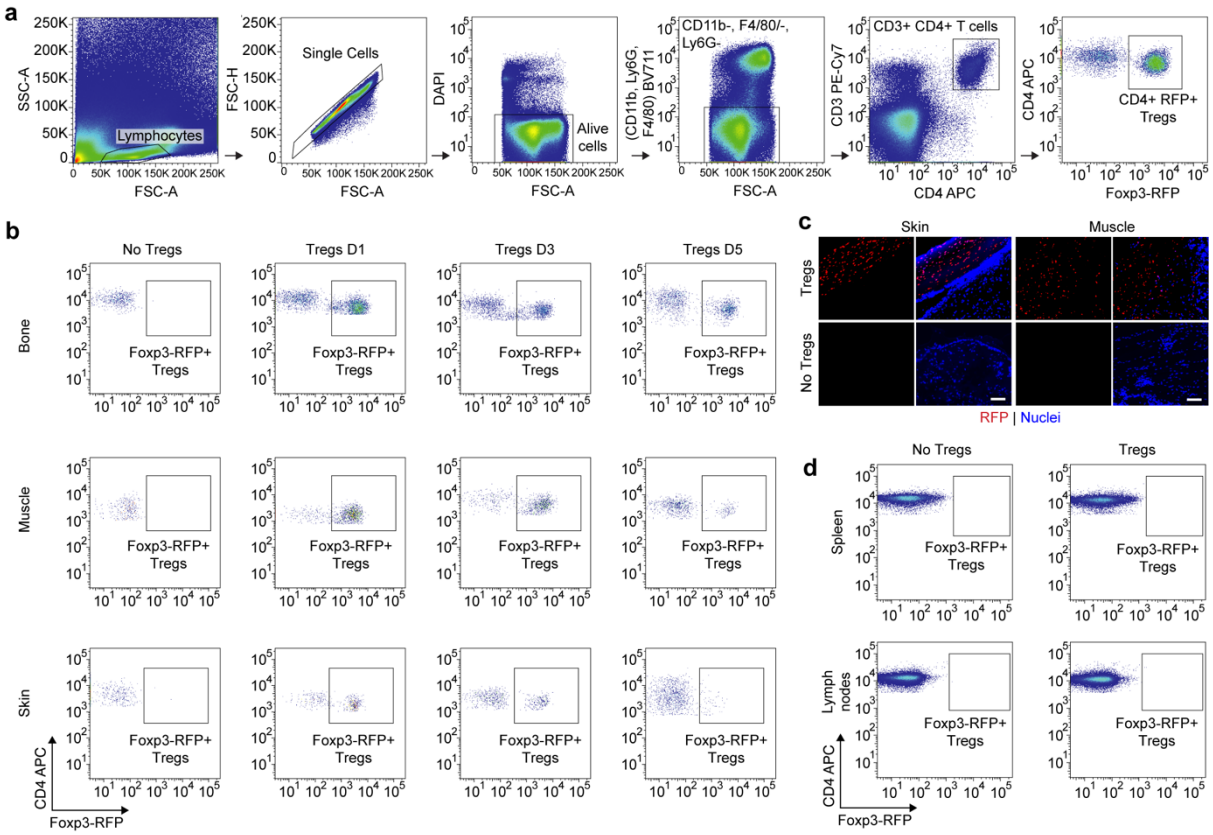

Supplementary Fig. 5: Representative flow cytometry plots for analysis of recovered exogenous RFP$^+$ Tregs from injured tissues following delivery. a, Gating strategy for detecting exogenous RFP$^+$ Tregs recovered from Treg-treated injured tissues (shown for muscle as an example). Exogenous Tregs were gated as CD4$^+$ RFP$^+$ Tregs from CD3$^+$ T cells, after excluding potential contaminating myeloid cells (CD11b$^+$, F4/80$^+$ and Ly6G$^+$ cells). **b**, Representative flow cytometry plots of RFP$^+$ Tregs recovered from the Treg-treated bone, muscle, and skin tissues, at D1, D3 and D5 post-injury, compared to untreated controls. **c**, Representative immunostaining of injured muscle and skin sections with endogenous RFP in red (Tregs) and nuclei in blue, at D3 post-injury for tissues administered with exogenous Tregs and controls (No Tregs). Scale bar: 100 µm. **d**, Representative flow cytometry plots of spleens and lymph nodes from all tissue injuries showing no presence of RFP$^+$ Tregs. (RFP: Red fluorescent protein).

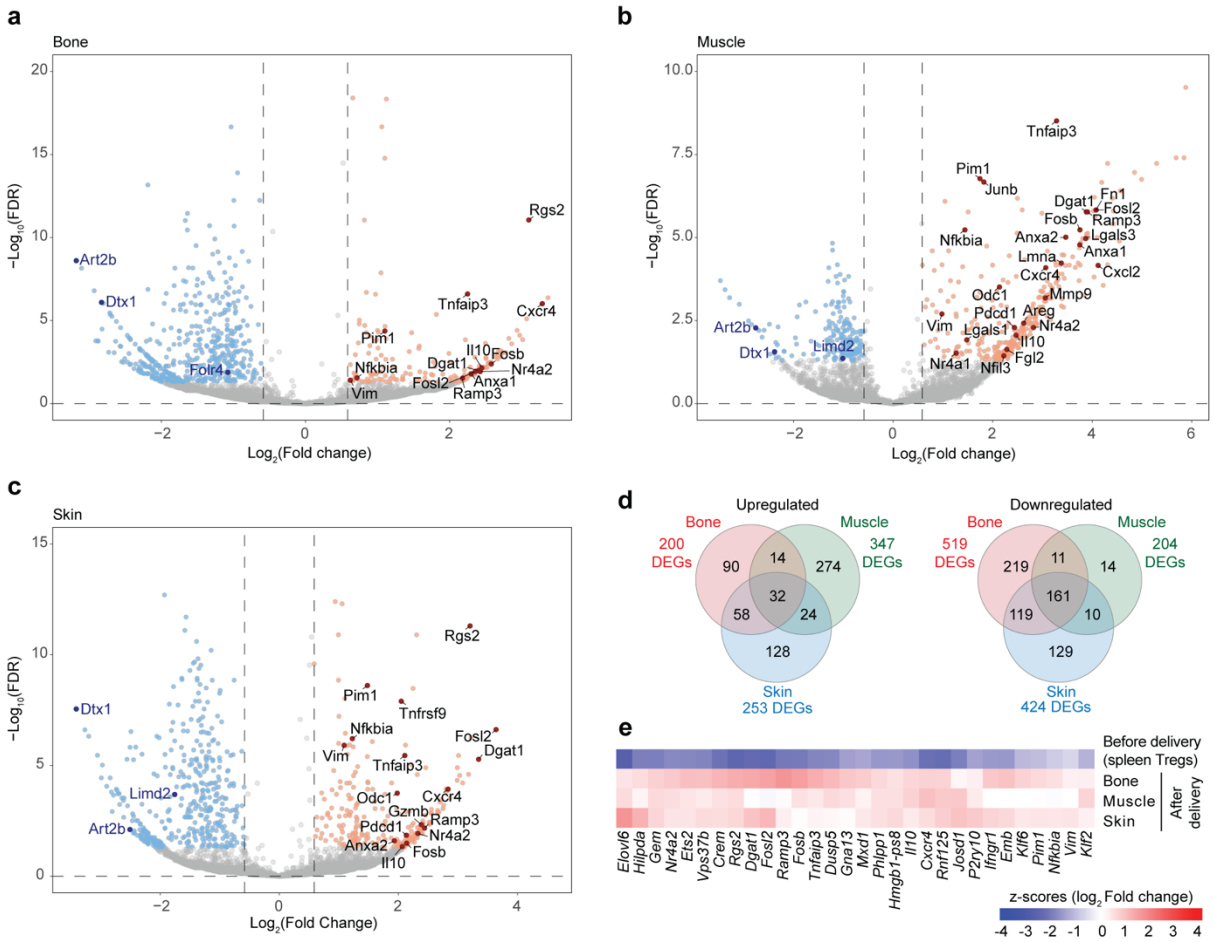

Supplementary Fig. 6: Differential gene expression analysis results of RNA-seq on exogenous Tregs before and after delivery into injured tissues. a-e, Critical-size cranial defects, quadriceps volumetric muscle loss defect or full-thickness dorsal skin wounds were performed in wildtype C57BL6/J mice, and treated with a fibrin hydrogel only, or hydrogel containing exogenous spleen Tregs. On D3 post-delivery, exogenous Tregs were sorted from injured bone, muscle, and skin for RNA sequencing. **a-c**, Volcano plots depicting differentially expressed genes (DEGs) (FDR adjusted p-value < 0.0.5, with fold change > |1.5|) between exogenous spleen Tregs before delivery (*n* = 4) and exogenous Tregs recovered from injured tissues at D3 post-delivery (*n* = 3) for bone (**a**), muscle (**b**) and skin (**c**). Significantly upregulated (red) and downregulated (blue) genes in D3 recovered Tregs are shown with key selected genes labelled. **d**, Venn diagrams depicting the overlapping number of DEGs between tissues for the upregulated and downregulated genes in exogenous Tregs recovered from injured tissues at D3 post-delivery compared to exogenous Tregs before delivery. **e**, Heat map depicting standardised expression values of the 32 upregulated DEGs that overlap between bone, muscle and skin (from **d**) (*n* = 4 mice for spleen Tregs before delivery and *n* = 3 mice per injured tissue after delivery; average of replicates is shown).

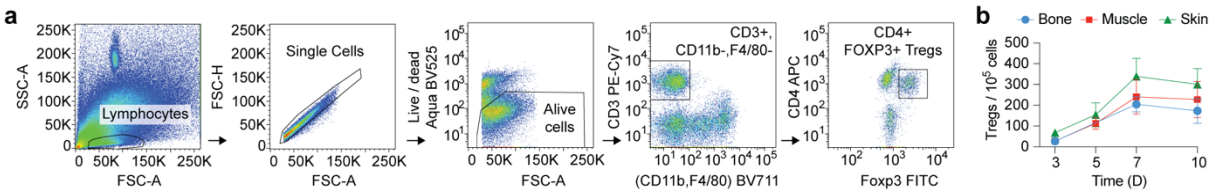

Supplementary Fig. 7: Kinetics of endogenous Treg accumulation in injured tissues. a, Gating strategy for detecting FOXP3$^+$ Tregs in injured bone, muscle, and skin of wildtype C57BL6/J mice by flow cytometry (shown for muscle as an example). **b**, Number of Tregs accumulating at different time points in each injured tissue. Data are plotted as mean ± SD (*n* = 5 mice per time point).

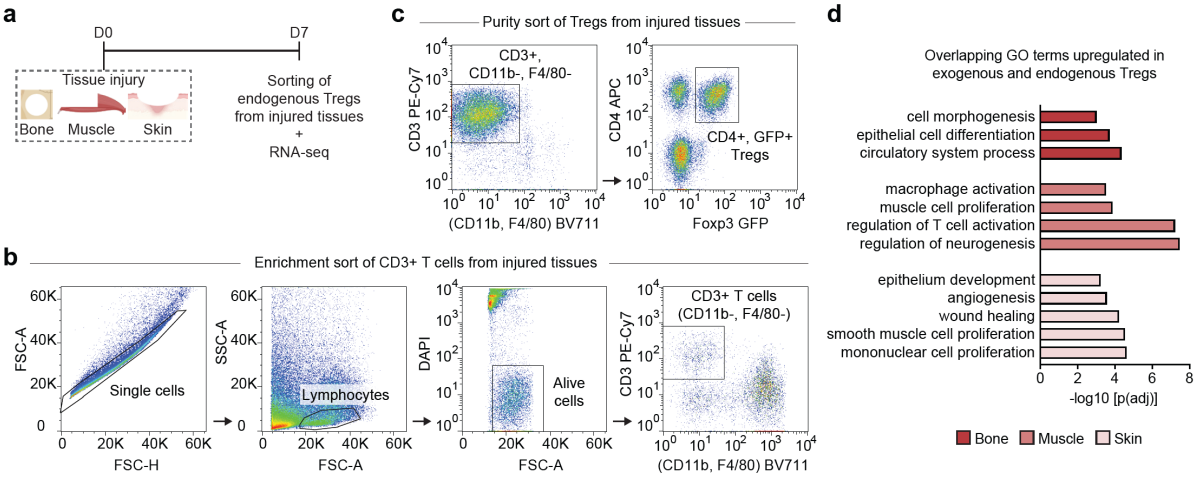

Supplementary Fig. 8: Characterising endogenous and exogenous Tregs in injured bone, muscle, and skin tissues. a, Endogenous Tregs were sorted from critical-size cranial defects, quadriceps volumetric muscle loss defect or full-thickness dorsal skin wounds of *Foxp3*$^{DTR/GFP}$ mice on D7 post-injury for RNA sequencing. **b-c**, Two-step sorting strategy for isolating endogenous Tregs from injured tissues (shown for muscle as an example), involving exclusion of contaminating CD11b^{+}, F4/80^{+} cells, while enriching for CD3^{+} T cells (**b**) followed by a purity sort for CD4^{+}, FoxP3-GFP^{+} Tregs. **d**, The transcriptome of sorted endogenous Tregs was compared to sorted exogenous Tregs and gene ontology analysis was performed on differentially expressed genes that were commonly upregulated between endogenous and exogenous Tregs sorted from the injured tissues. Panel (**a**) created with BioRender.com released under a Creative Commons Attribution-NonCommercial-NoDerivs 4.0 International license (https://creativecommons.org/licenses/by-nc-nd/4.0/deed.en).

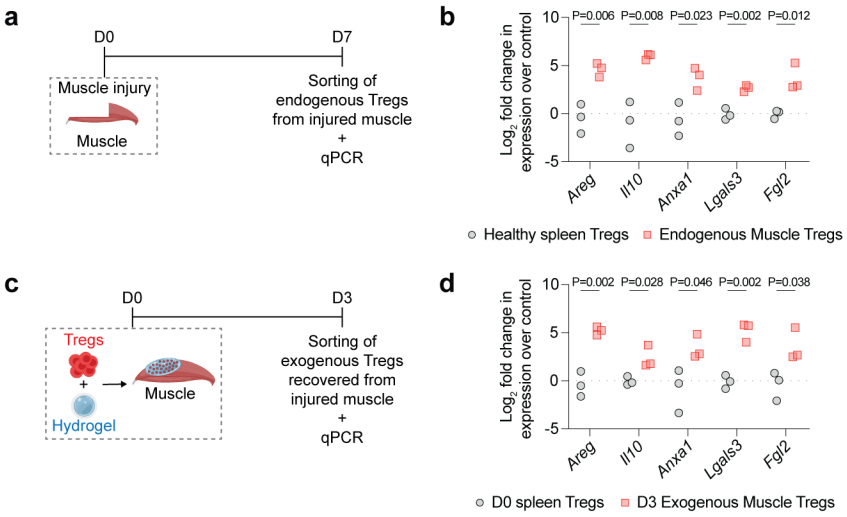

Supplementary Fig. 9: RT-qPCR analysis of selected genes significantly upregulated in RNA-seq data of endogenous and exogenous Tregs from injured muscle compared to healthy spleen Tregs. a-b, Endogenous Tregs were sorted from quadriceps volumetric muscle loss defects of *Foxp3*$^{DTR/GFP}$ mice on D7 post-injury for RT-qPCR, *n* = 3 per group. **c-d**, Quadriceps volumetric muscle loss defects were performed in wildtype C57BL6/J mice, and treated with a fibrin hydrogel only, or hydrogel containing exogenous spleen Tregs. On D3 post-delivery, exogenous Tregs were sorted from injured muscle for RT-qPCR, *n* = 3 per group. Data in **b**, **d** are expressed as Log_2 fold change in expression of each gene in Tregs from injured muscle, compared to Tregs from healthy spleen. Panels (**a, c**) created with BioRender.com released under a Creative Commons Attribution-NonCommercial-NoDerivs 4.0 International license (https://creativecommons.org/licenses/by-nc-nd/4.0/deed.en).

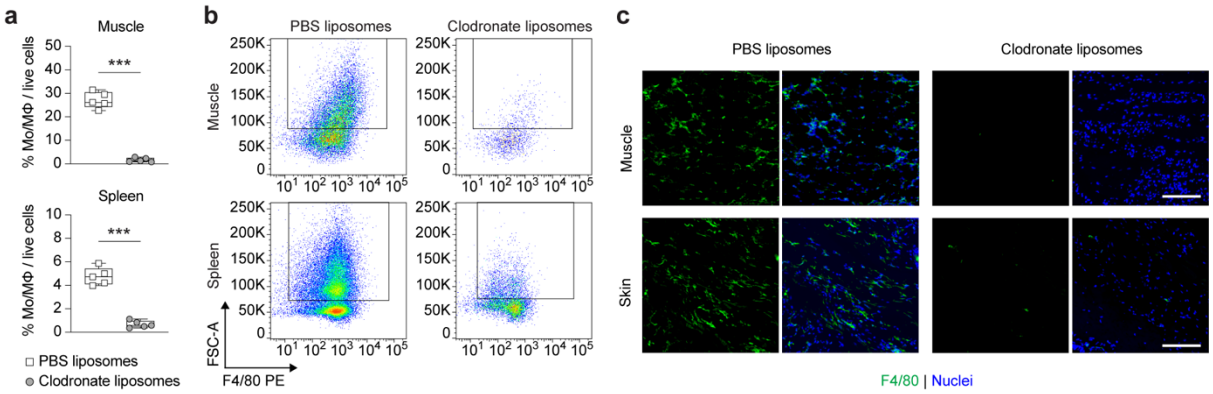

Supplementary Fig. 10: Validating Mo/MΦ depletion with clodronate liposomes. **a-c,** Mice received PBS liposomes or clodronate liposomes via intraperitoneal injection, starting one day prior to quadriceps volumetric muscle loss injury. Macrophage populations in muscle and spleen from injured mice were analysed via flow cytometry (**a-b**) and immunostaining (**c**) for F4/80 on D4 post-injury. Data in (**a**) are plotted in box plots showing the median (central line) and IQR (bounds) with whiskers extending to the minimum and maximum values. Two-tailed unpaired Student's *t*-test was used. *P* values are indicated; ***$P \leq 0.001$. (**b**) Representative flow cytometry plots of muscle and spleen macrophages ($F4/80^+$ cells). (**c**) Representative immunostaining of injured muscle and skin sections for F4/80 in green (macrophages) and nuclei in blue at D4 post-injury. Scale bar: 100 µm. (Mo/MΦ: monocytes/ macrophages).

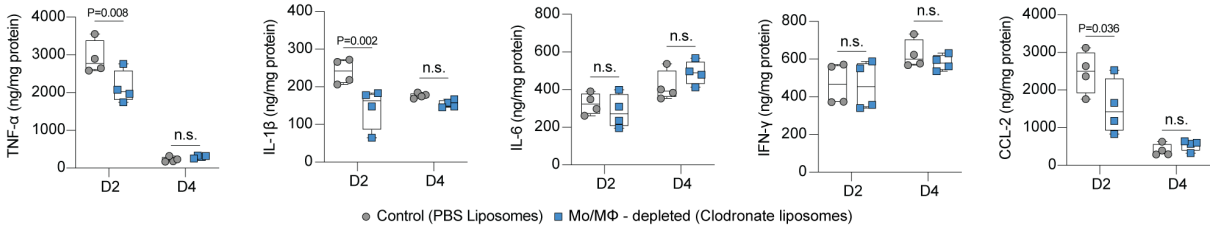

Supplementary Fig. 11: Mice received PBS liposomes or clodronate liposomes via intraperitoneal injection, starting one day prior to quadriceps volumetric muscle loss injury. The levels of TNF-α, IL-1β, IL-6, IFN-γ and CCL-2 within the injured muscle tissue were quantified by ELISA (*n* = 4) on D2 and D4 post-injury. Data are plotted in box plots showing the median (central line) and IQR (bounds) with whiskers extending to the minimum and maximum values. Two-tailed unpaired Student's *t*-test was used for each time point. *P* values are indicated; n.s indicates non-significant. (Mo/MΦ: monocytes/ macrophages).

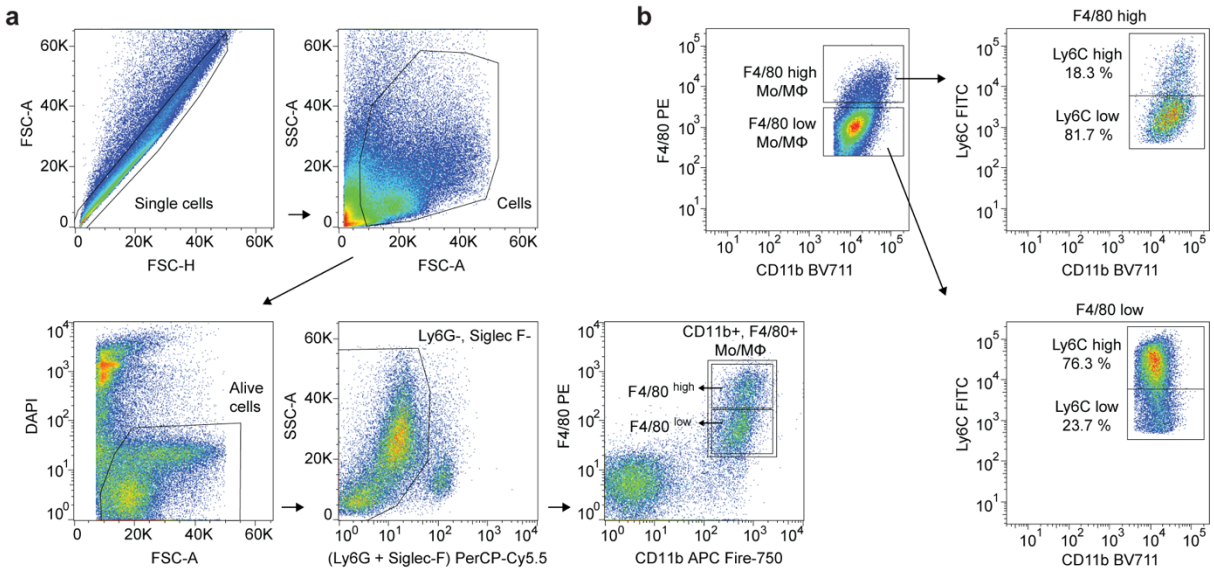

Supplementary Fig. 12: Isolating tissue Mo/MΦ from injured tissues. a, Representative flow cytometry gating strategy for sorting endogenous Mo/MΦ from injured bone, muscle, and skin tissues (shown here for skin as an example), by excluding Ly6G$^+$ neutrophils, and Siglec-F$^+$ eosinophils, before gating for CD11b$^+$, F4/80$^+$ cells. **b**, Expression of Ly6C within the F4/80 high/low subsets demonstrating the inverse correlation in the expression of these markers.

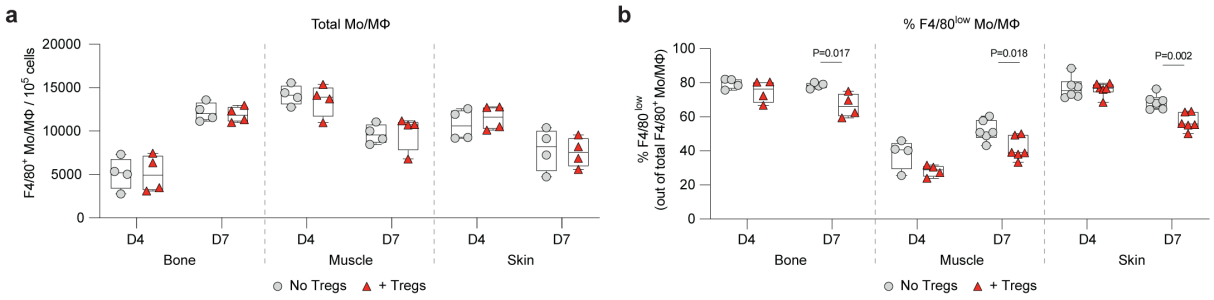

Supplementary Fig. 13: Dynamics of Mo/MΦ accumulation in Treg-treated and wildtype C57BL/J control mice on D4 and D7 post-injury. Number of F4/80$^+$ Mo/MΦ per 10^5 cells in (**a**) and percentages of the F4/80 low fraction within the total F4/80$^+$ Mo/MΦ population sorted from injured tissues in (**b**) (*n* = 4 mice per time point). Data are plotted in box plots showing the median (central line) and IQR (bounds) with whiskers extending to the minimum and maximum values. Two-tailed unpaired Student's *t*-test was used for pairwise comparisons between Treg-treated and untreated groups within each time point. *P* values are indicated. (Mo/MΦ: monocytes/ macrophages).

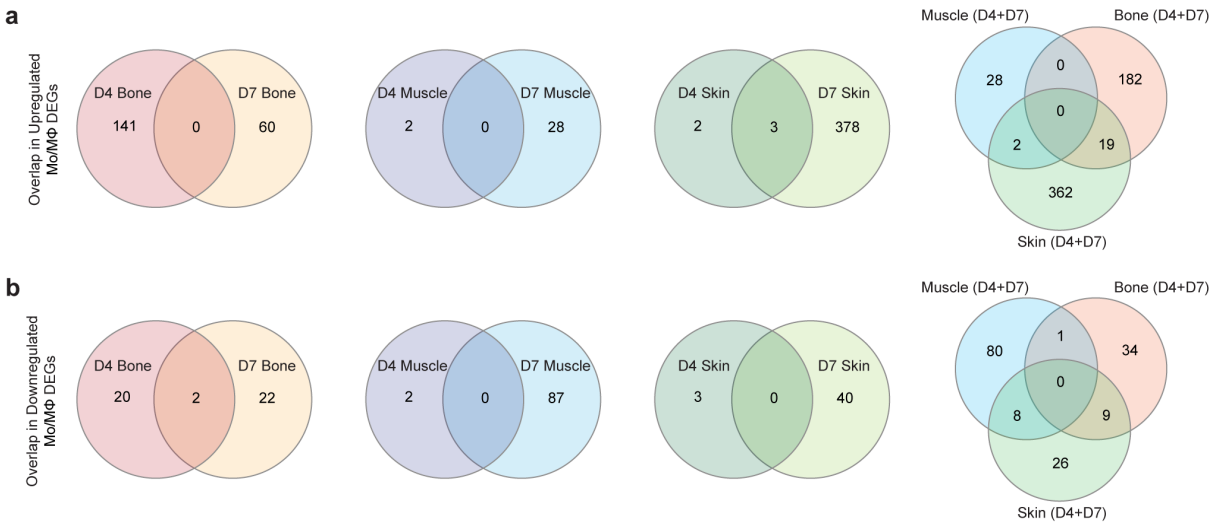

Supplementary Fig. 14: Venn diagrams depicting the overlap of DEGs between Mo/MΦ from Treg-treated tissues sorted at D4 and D7 post-injury. Wildtype C57BL6/J mice with bone, muscle or skin injuries were treated with fibrin hydrogel only or hydrogel containing exogenous Tregs. Endogenous Mo/MΦ from injured tissues were sorted for RNA sequencing on D4 and D7 post-injury. Overlapping number of genes between all significantly upregulated (**a**) and downregulated (**b**) differentially expressed genes (DEGs) (FDR adjusted p-value < 0.05) is shown. (Mo/MΦ: monocytes/ macrophages).

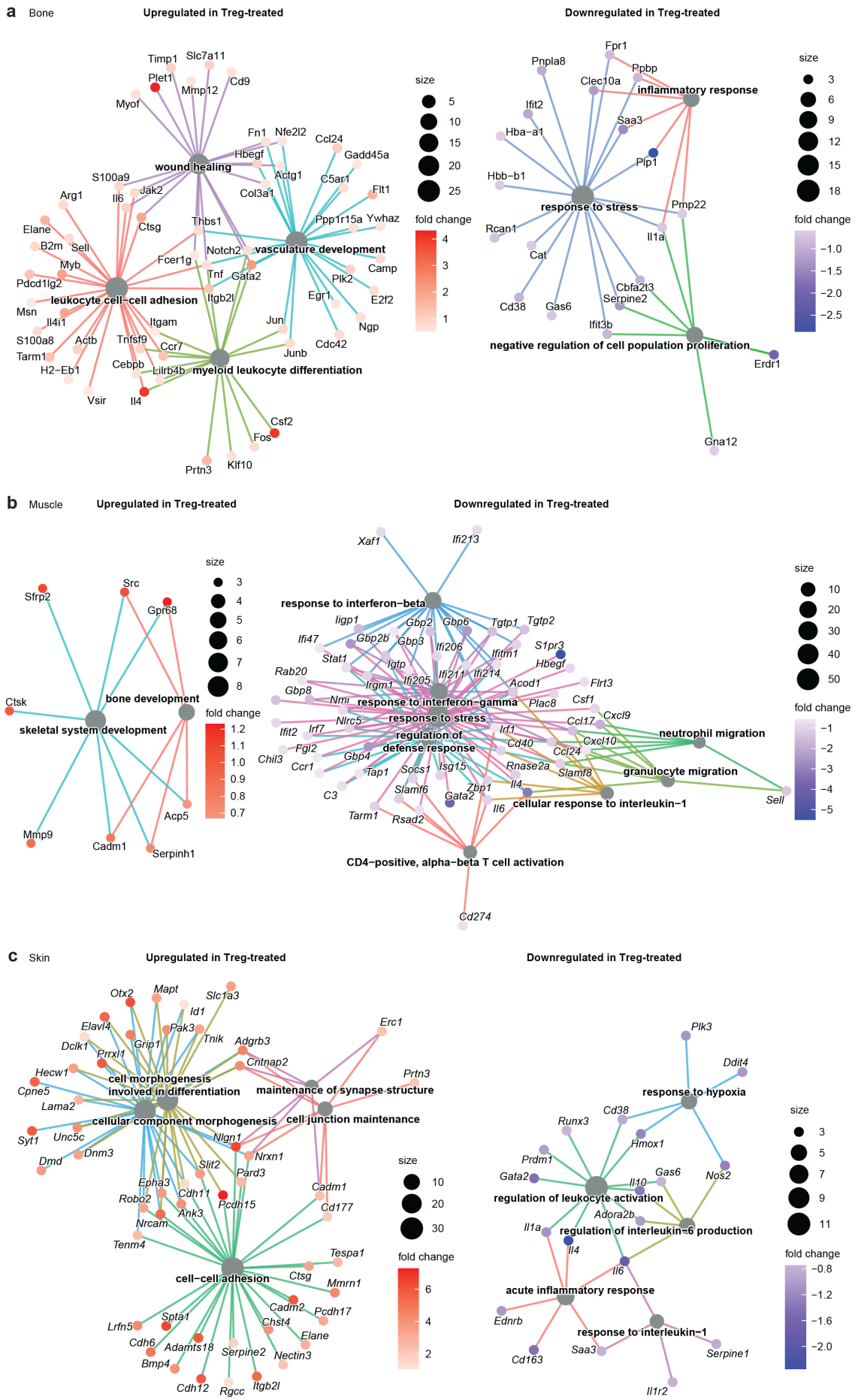
a
Bone
Upregulated in Treg-treated
Downregulated in Treg-treated
wound healing
vasculature development
leukocyte cell−cell adhesion
myeloid leukocyte differentiation
inflammatory response
response to stress
negative regulation of cell population proliferation
b
Muscle
Upregulated in Treg-treated
Downregulated in Treg-treated
bone development
skeletal system development
response to interferon−beta
response to interferon−gamma
response to stress
regulation of defense response
neutrophil migration
granulocyte migration
cellular response to interleukin−1
CD4−positive, alpha−beta T cell activation
c
Skin
Upregulated in Treg-treated
Downregulated in Treg-treated
cell morphogenesis involved in differentiation
cellular component morphogenesis
maintenance of synapse structure
cell junction maintenance
cell−cell adhesion
response to hypoxia
regulation of leukocyte activation
regulation of interleukin−6 production
acute inflammatory response
response to interleukin−1
size
fold change

Supplementary Fig. 15: Gene-concept network plot of top gene ontology processes enriched in Mo/MΦ from injured bone, muscle, and skin of Treg-treated mice. Network of the top gene ontology (GO) biological processes (with adjusted $P < 0.01$; Bonferroni correction) enriched in the differentially expressed upregulated and downregulated Mo/MΦ genes combined from both D4 and D7 post-injury, for Treg-treated bone (**a**), muscle (**b**) and skin (**c**). The circle size represents the number of genes associated with the term and fold change indicates expression levels with red colour depicting upregulation and blue colour representing downregulation. The individual colours of the lines within the gene network depict individual GO terms. (Mo/MΦ: monocytes/ macrophages).

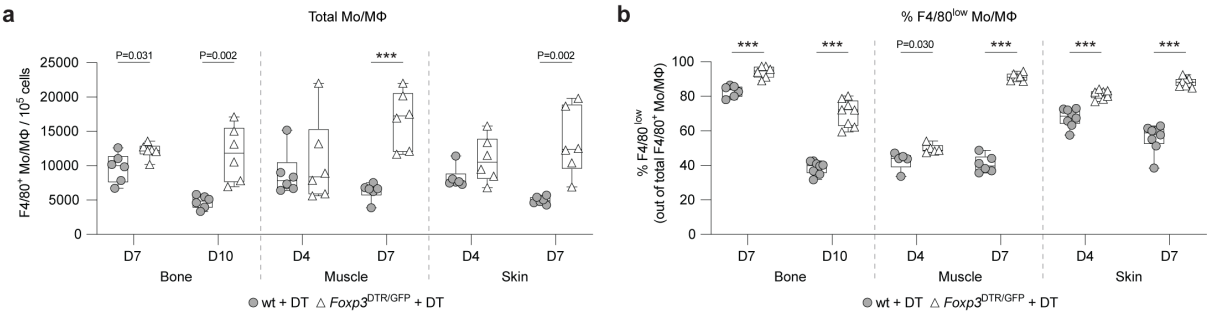

Supplementary Fig. 16: Dynamics of Mo/MΦ accumulation in Treg-depleted and control mice on D4 and D7 post-injury. Number of F4/80$^+$ Mo/MΦ per 10^5 cells in (**a**) and percentages of the F4/80 low fraction within the total F4/80$^+$ Mo/MΦ population sorted from injured tissues in (**b**). *n* = 6 mice per time point in (**a**) and *n* = 5 – 8 mice per time point in (**b**). Data are plotted in box plots showing the median (central line) and IQR (bounds) with whiskers extending to the minimum and maximum values. Two-tailed unpaired Student's *t*-test was used for pairwise comparisons between Treg-depleted and control groups within each time point. *P* values are indicated, ***$P \leq 0.001$. (Mo/MΦ: monocytes/ macrophages).

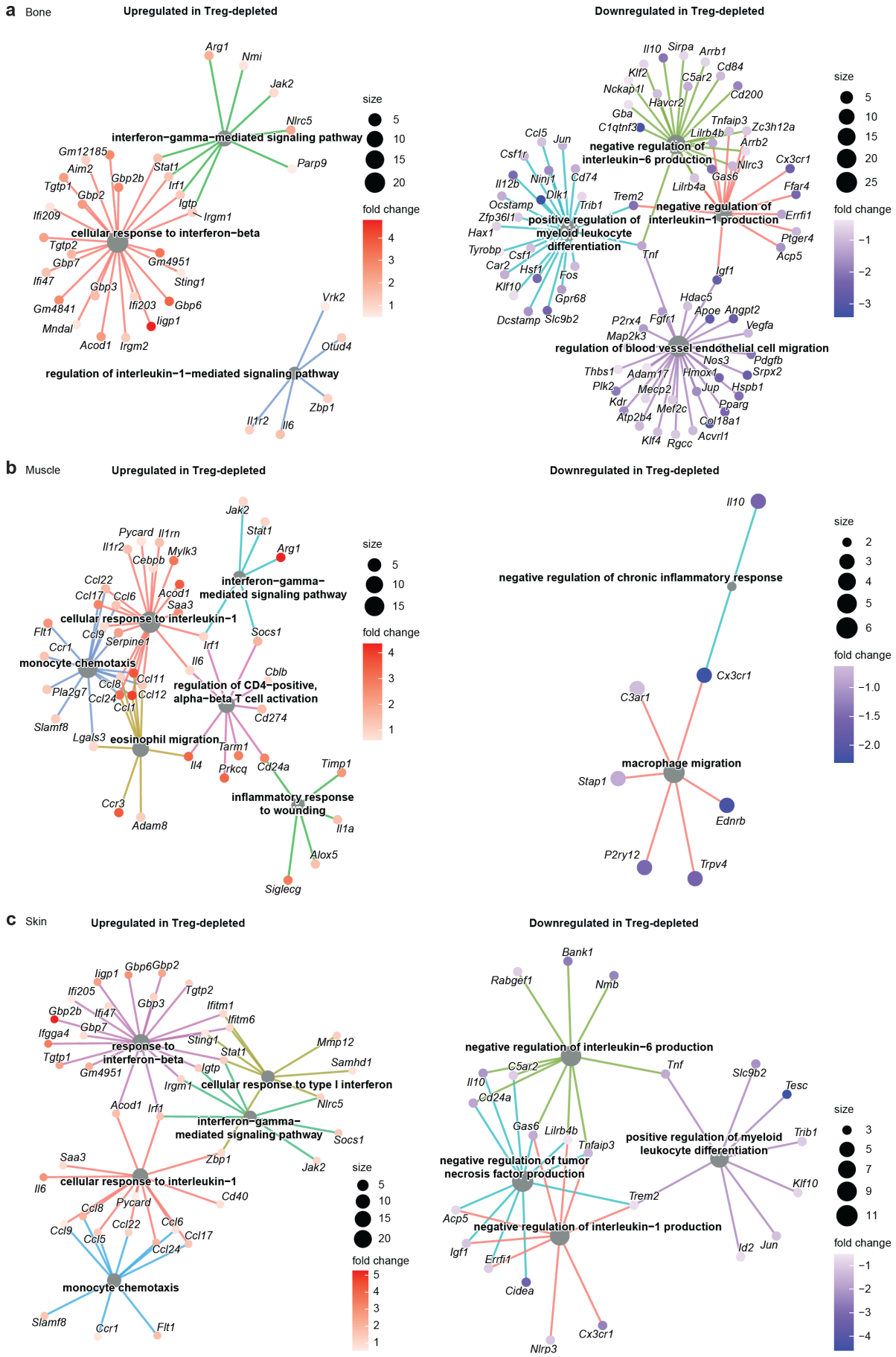
a Bone
Upregulated in Treg-depleted
Downregulated in Treg-depleted
b Muscle
Upregulated in Treg-depleted
Downregulated in Treg-depleted
c Skin
Upregulated in Treg-depleted
Downregulated in Treg-depleted
size
fold change
interferon−gamma−mediated signaling pathway
cellular response to interferon−beta
regulation of interleukin−1−mediated signaling pathway
negative regulation of interleukin−6 production
negative regulation of interleukin−1 production
positive regulation of myeloid leukocyte differentiation
regulation of blood vessel endothelial cell migration
negative regulation of chronic inflammatory response
macrophage migration
cellular response to interleukin−1
monocyte chemotaxis
regulation of CD4−positive, alpha−beta T cell activation
eosinophil migration
inflammatory response to wounding
response to interferon−beta
cellular response to type I interferon
negative regulation of tumor necrosis factor production

Supplementary Fig. 17: Gene-concept network plot of top gene ontology processes enriched in Mo/MΦ from injured bone, muscle, and skin of Treg-depleted mice. Network of the top gene ontology (GO) biological processes (with adjusted $P < 0.01$; Bonferroni correction) enriched in the differentially expressed upregulated and downregulated Mo/MΦ genes combined from both time points post-injury, for Treg-depleted bone (**a**), muscle (**b**) and skin (**c**) (D4 and D7 for skin and muscle; D7 and D10 for bone). The circle size represents the number of genes associated with the term and fold change indicates expression levels with red colour depicting upregulation and blue colour representing downregulation. The individual colours of the lines within the gene network depict individual GO terms. (Mo/MΦ: monocytes/ macrophages).

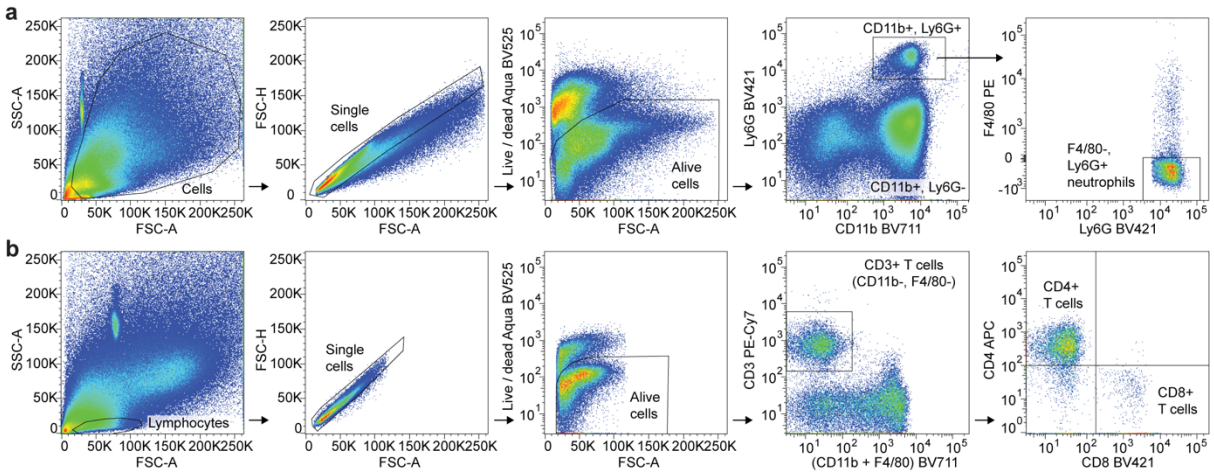

Supplementary Fig. 18: Flow cytometry gating strategies for analysing endogenous neutrophils and T cells in Treg-treated injured tissues. a, Gating strategy for analysing neutrophils from $CD11b^+$ myeloid cells post-injury, as the $Ly6G^+$, $F4/80^-$ population. **b**, Gating strategy for analysing T cells post-injury. Total $CD3^+$ T cells were gated by excluding $CD11b^+$, $F4/80^+$ Mo/MΦ, followed by subsequent gating for $CD8^+$ and $CD4^+$ T cells. Plots have been shown for muscle injury as an example.

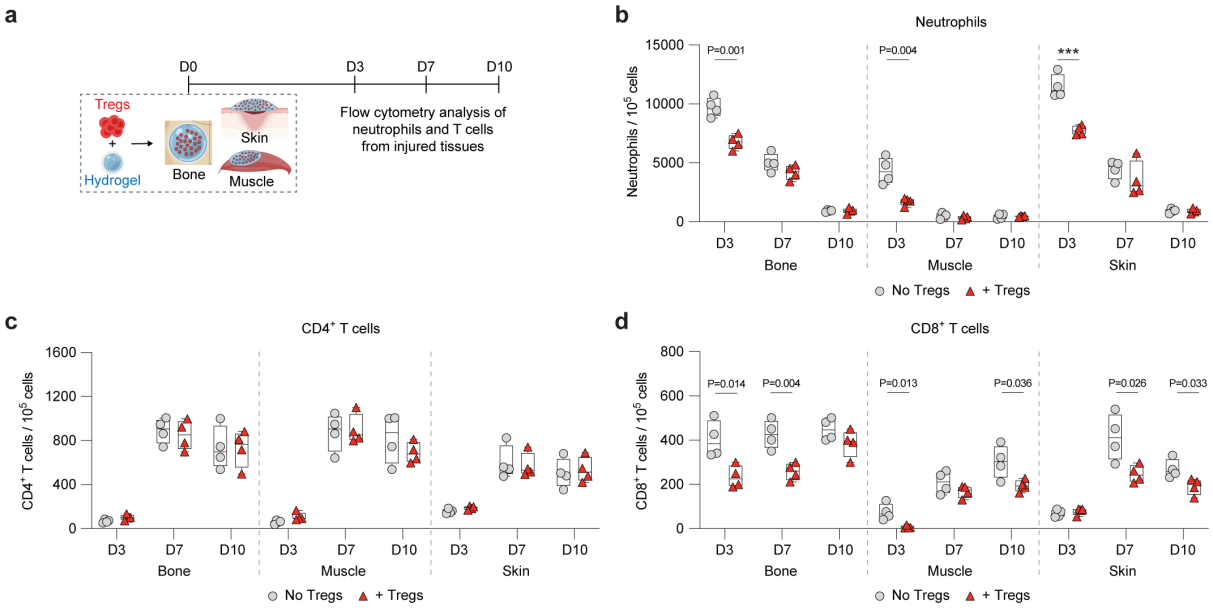

Supplementary Fig. 19: Kinetics of neutrophil and T cell accumulation in injured bone, muscle, and skin, following Treg delivery. a, Wildtype C57BL/6J mice with critical-size cranial defects, quadriceps volumetric muscle loss defect or full-thickness dorsal skin wounds were treated with a fibrin hydrogel only, or hydrogel containing exogenous spleen Tregs. Endogenous neutrophils and T cells accumulating in the injured tissues were analysed by flow cytometry on D3, D7 and D10 post-injury. **b-d**, Numbers of neutrophils ($CD11b^+$, $Ly6G^+$, $F4/80^-$) (**b**), $CD4^+$ T cells ($CD3^+$, $CD4^+$) (**c**) and $CD8^+$ T cells ($CD3^+$, $CD8^+$) (**d**) in injured tissues per 10^5 live cells (n = 4 mice per time point). Data are plotted in box plots showing the median (central line) and IQR (bounds) with whiskers extending to the minimum and maximum values. Two-tailed unpaired Student's t-test was used for pairwise comparisons between Treg-treated and untreated groups within each time point. P values are indicated; $^{***}P \leq 0.001$. Panel (**a**) created with BioRender.com released under a Creative Commons Attribution-NonCommercial-NoDerivs 4.0 International license (https://creativecommons.org/licenses/by-nc-nd/4.0/deed.en).

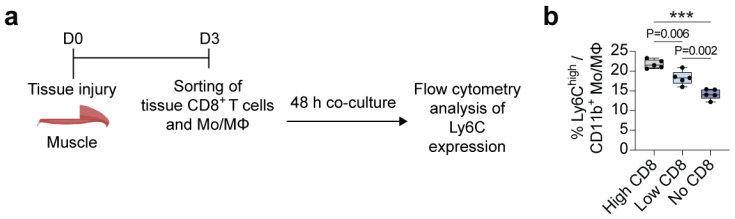

Supplementary Fig. 20: Co-culture of Mo/MΦ with decreasing concentrations of cytotoxic T cells decreases their pro-inflammatory phenotype. a-b, Volumetric muscle loss defects were created and endogenous $CD8^+$ T cells and Mo/MΦ were sorted on D3 post-injury, followed by a 48 h co-culture of Mo/MΦ with different concentrations of $CD8^+$ T cells (**a**). The proportions of $Ly6C^{high}$ Mo/MΦ within each condition were quantified (**b**) (n = 5 biological replicates). Data in (**b**) are plotted in box plots showing the median (central line) and IQR (bounds) with whiskers extending to the minimum and maximum values. One-way ANOVA with Bonferroni *post hoc* test was used in (**b**) for multiple comparisons. P values are indicated; $^{***}P \leq 0.001$. (Mo/MΦ: monocytes/ macrophages). Panel (**a**) created with BioRender.com released under a Creative Commons Attribution-NonCommercial-NoDerivs 4.0 International license (https://creativecommons.org/licenses/by-nc-nd/4.0/deed.en).

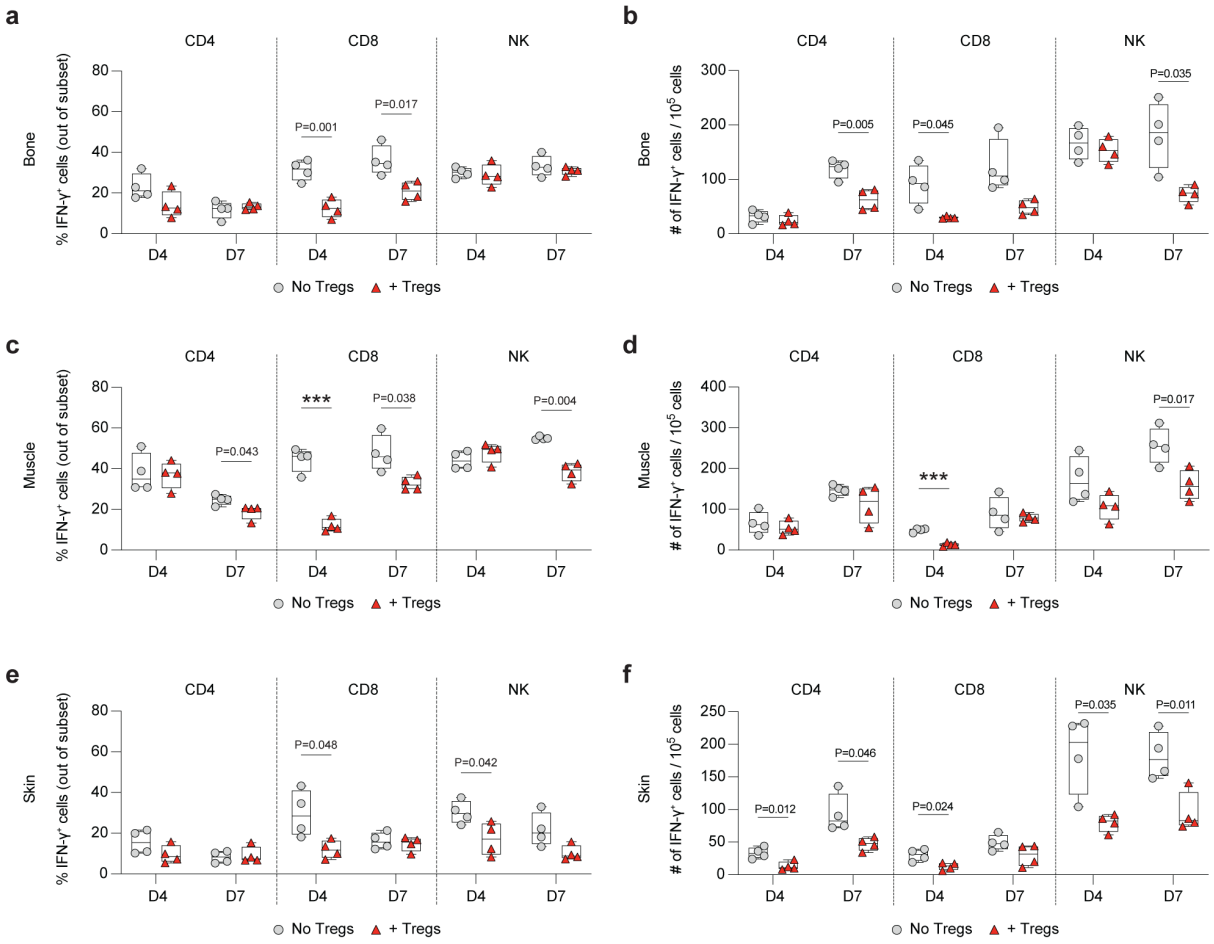

Supplementary Fig. 21: Kinetics of IFN-γ$^+$ T cell and NK cell accumulation in injured bone, muscle, and skin, following Treg delivery. a, Wildtype C57BL/6J mice with critical-size cranial defects, quadriceps volumetric muscle loss defect or full-thickness dorsal skin wounds were treated with a fibrin hydrogel only, or hydrogel containing exogenous spleen Tregs. Expression of IFN-γ in endogenous CD4$^+$ T cells, CD8$^+$ T cells and NK cells accumulating in the injured tissues were analysed by flow cytometry on D4 and D7 post-injury. Percentages within each subset are shown in **a**, **c, e**. Number of cells per 10^5 live cells is shown in **b**, **d**, **f**. (*n* = 4 mice per time point). Data are plotted in box plots showing the median (central line) and IQR (bounds) with whiskers extending to the minimum and maximum values. Two-tailed unpaired Student's *t*-test was used for pairwise comparisons between Treg-treated and untreated groups within each time point. *P* values are indicated; ***$P \leq 0.001$.

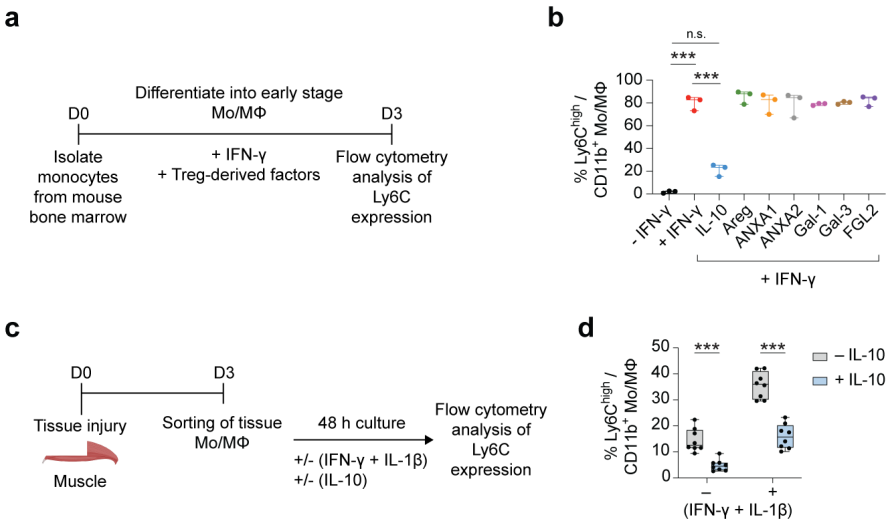

Supplementary Fig. 22: IL-10 decreases the pro-inflammatory phenotype of injured muscle Mo/MΦ. a-b, Monocytes were isolated from mouse bone marrow and cultured for 3 days with Treg-derived factors in the presence of IFN-γ. The proportion of Ly6C^{high} Mo/MΦ was measured by flow cytometry (n = 3 biological replicates). Data in (**b**) are plotted as mean ± SD and data points represent independent pools of mouse monocyte culture. One-way ANOVA with Bonferroni *post hoc* test was used in (**b**) for multiple comparisons. **c-d**, Volumetric muscle loss defects were created and endogenous Mo/MΦ were sorted on D3 post-injury, followed by a 48 h culture, with and without IFN-γ and IL-1β, in the presence or absence of IL-10. The proportions of Ly6C^{high} Mo/MΦ within each condition were measured by flow cytometry (n = 8 biological replicates). Data in (**d**) are plotted in box plots showing the median (central line) and IQR (bounds) with whiskers extending to the minimum and maximum values. Two-tailed unpaired Student's *t*-test was used for pairwise comparisons between untreated and IL-10-treated groups within each condition (with and without IFN-γ and IL-1β) in (**d**). *P* values are indicated; ***$P \leq 0.001$; n.s. indicates non-significant. (Mo/MΦ: monocytes/ macrophages). Panel (**c**) created with BioRender.com released under a Creative Commons Attribution-NonCommercial-NoDerivs 4.0 International license (https://creativecommons.org/licenses/by-nc-nd/4.0/deed.en).

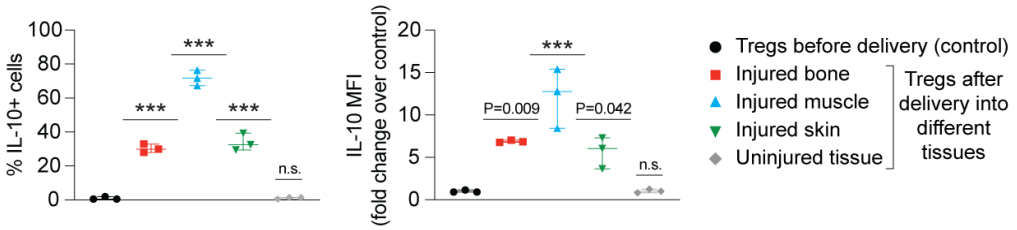

Supplementary Fig. 23: Exogenous Tregs express IL-10. Wildtype C57BL/6J mice with cranial bone defects, quadriceps volumetric muscle loss defects, or dorsal skin wounds were treated with a fibrin hydrogel containing exogenous spleen Tregs, while for uninjured tissue, Tregs were placed within a small pocket formed in the subcutaneous space by blunt dissection. The delivered exogenous Tregs were recovered from injured tissue by sorting on D3 post-injury and IL-10 expression was measured by flow cytometry, represented as the percentage of IL-10$^+$ Tregs or the mean fluorescence intensity (MFI) of IL-10 expression in the sorted Tregs, before and after delivery into injured tissues (n = 3 mice per group). Data are plotted as mean ± SD and data points represent individual mice. One-way ANOVA with Bonferroni *post hoc* test was used for multiple comparisons. P values are indicated; ***$P \leq 0.001$; n.s. indicates non-significant.

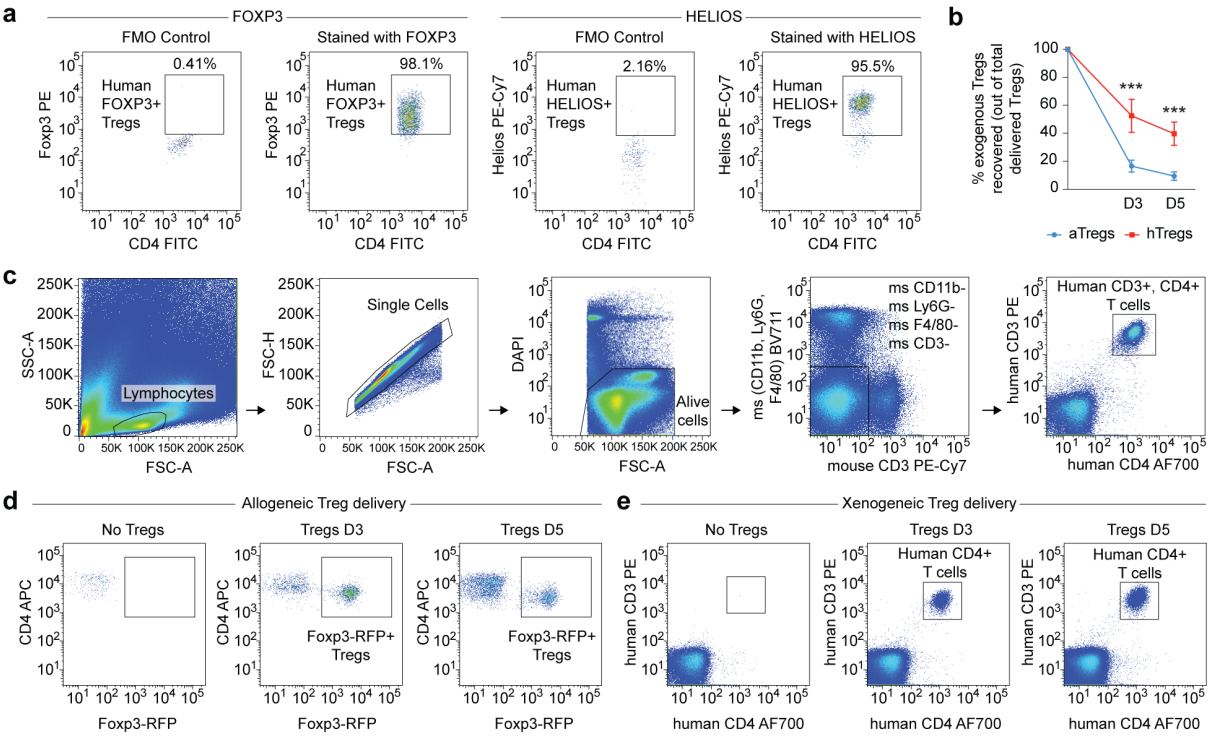

Supplementary Fig. 24: Purity of human Tregs prior to delivery and recovery of exogenous allogeneic and human Tregs from injured bone following delivery. a, Expression of FOXP3 and HELIOS in the *in vitro* expanded and cryopreserved human Tregs after thawing prior to *in vivo* delivery (gated on live human $CD4^+$ Tregs). **b**, Percentage of exogenous allogeneic and human Tregs recovered from injured bone, on D3 and D5 post-Treg delivery (data are mean ± SD, $n = 4$ mice), $^{***}P \leq 0.001$. **c**, Gating strategy for recovering exogenous human Tregs from Treg-treated injured bone. Exogenous human Tregs were gated by first excluding potential contaminating myeloid cells ($CD11b^+$, $F4/80^+$, $Ly6G^+$ cells) as well as mouse $CD3^+$ T cells, followed by selecting human $CD3^+$, $CD4^+$ T cells. **d-e**, Representative flow cytometry plots of recovered RFP^+ Tregs after allogeneic delivery (**d**) or recovered $CD4^+$ human Tregs after xenogeneic delivery (**e**) from the Treg-treated bone at D3 and D5 post-injury, compared to untreated controls. (aTregs: allogeneic Tregs; hTregs: human Tregs).

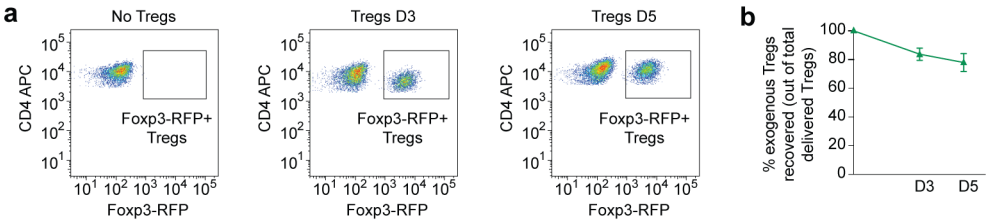

Supplementary Fig. 25: Recovering exogenous Tregs, with prior *in vitro* culture, from injured bone following delivery. a, Representative flow cytometry plots of recovered RFP^+ Tregs after delivery into injured bone. **b**, Percentage of exogenous Tregs recovered from injured bone, on D3 and D5 post-Treg delivery (data are mean ± SD, *n* = 4 mice).

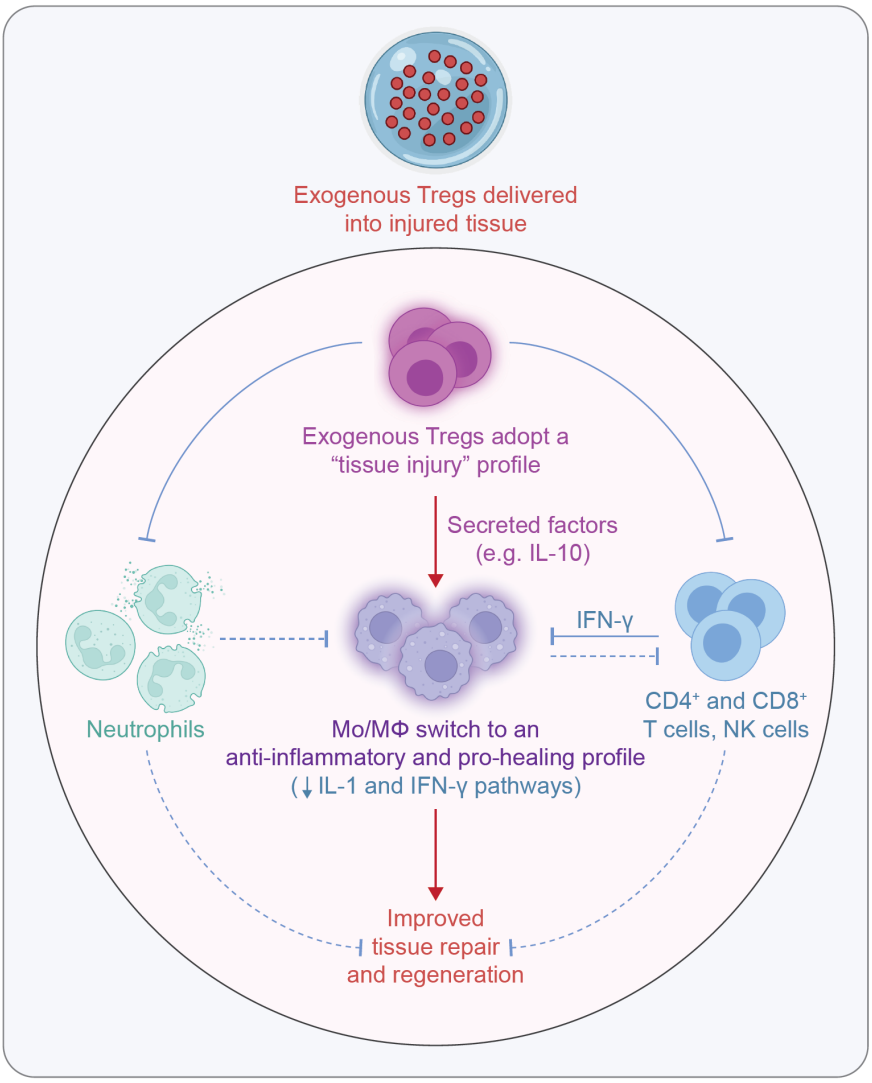

Supplementary Fig. 26: Proposed mechanisms by which local delivery of exogenous Tregs into injured tissues promotes healing. Tregs delivered locally into injured tissues respond to the microenvironment and adopt an "injury-specific" phenotype characterised by the expression of effector molecules. Exogenous Tregs rapidly modulate other immune cells within the injured site, particularly Mo/MΦ via IL-10 and potentially other Treg-derived factors, promoting their polarisation to an anti-inflammatory and pro-healing state. Additionally, exogenous Tregs affect the immune microenvironment by reducing the number of neutrophils and cytotoxic $CD8^+$ T cells, as well as IFN-γ-producing T cells and NK cells, further contributing to Mo/MΦ polarisation. The timely modulation of the immune response by exogenous Tregs, following acute injury, leads to an overall improved tissue healing outcome. Red arrows indicate induction and blue arrows indicate inhibition. Dotted arrows indicate proposed interactions or effects. Figure created with BioRender.com released under a Creative Commons Attribution-NonCommercial-NoDerivs 4.0 International license (https://creativecommons.org/licenses/by-nc-nd/4.0/deed.en).